Bending Behavior of Separable Glued-Laminated Timber (GLT)-Steel Beam Combined with Inclined Screws

Sung-Jun Pang,[a] and Jung-Kwon Oh [a,b,*]

A separable glued-laminated timber (GLT, *Larix kaempferi* Carr.)-steel beam system is presented in this work for easy recycling at the time of disposal. The minimum thickness of steel required to induce compressive GLT failure was assembled with GLT by inclined screws. In a total of 8 GLTs, 3 GLTs were not reinforced (control group), and 5 GLTs were reinforced with steel plates (comparison group). In the GLT in the comparison group, a steel plate (SPHC, yield strength: 227 MPa, modulus of elasticity 166.33 GPa) was installed with screws (Ø9x160mm, 45°). The deflection and load of specimens were measured by a third-point bending test to derive their bending stiffness and load-carrying capacities. All specimens in the control group showed brittle tensile failure, but all specimens in the comparison group showed ductile behavior and maintained a load-carrying capacity of about 30 kN. After the compression failure of the GLT, there was no damage to the screw connection, while the steel plate was extended. Based on the behavior of the steel, a GLT-steel beam prediction model was developed, similar to the structural design method for reinforced concrete.

DOI: 10.15376/biores.18.2.3838-3855

Keywords: Glued-laminated timber; Steel; Composite beam; Bending performance; Reinforcement

*Contact information: a: Department of Agriculture, Forestry and Bioresources, Seoul National University, Seoul, Republic of Korea; b: Research Institute of Agriculture and Life Sciences, Seoul National University, Seoul, Republic of Korea; * Corresponding author: jungoh@snu.ac.kr*

INTRODUCTION

Carbon emission reduction has become a key topic in the construction industry. Timber construction has a low-carbon emission due to the light weight and easy cutting of the timber elements (Gerilla *et al*. 2007; Yan *et al*. 2010; Hafner and Schäfer 2018; Sandanayake *et al*. 2018; Li *et al*. 2019; Röck *et al*. 2020). In addition, timber retains carbon absorbed as the tree grows. Structural timber within a building will store the carbon as long as the building is maintained. Thus, the use of timber as a structural element contributes to the atmospheric carbon emissions reduction of buildings (Petersen Raymer 2006; Resch *et al*. 2021; Pang *et al*. 2022).

Structural timber is used as a beam due to its high bending strength compared to its weight. The design value of structural timber is based on the 5% lower limit, which is the 5th value from the lowest strength when 100 destructive tests are conducted (Pang *et al*. 2013, 2020). This is because a high safety factor is required for timber due to brittle failure. If the timber is subjected to ductile failure rather than brittle failure, then the safety factor can be lowered. Steel is a typical structural material with good ductility. The combination of steel and glued-laminated timber (GLT) is used in dry construction and the components are recyclable (Tsai and Le 2018). In addition, both materials are cut or drilled in the factory

using CNC cutting machines (Lee *et al*. 2021). Thus, the machining precision is high and the machining error is small (Tolerances: ±1mm range). This means that the two materials have many advantages that can be used as a hybrid.

Several researchers tried to develop timber-steel hybrid beams (Moritani *et al*. 2021). André (2006) showed that when the GLT is reinforced by steel, the bending performance of the GLT beam is improved and the deviation is reduced. Riola Parada (2016) showed that the creep of a GLT beam reinforced by steel was around 85% (after one year) and 50% (after the fifth year) of the GLT beam. Loss *et al*. (2016a, b) used an I-shape steel beam to avoid the brittle failure of the timber beam and timber floor in the fabrication of modern buildings. Tsai and Le (2018) reinforced the web of an I-shaped steel beam with timber using screws, and the strength of the composite beam was improved by about 15%. Wu *et al*. (2021) developed an I-shaped wood-steel composite beam and reported that an elastic-plastic phase appeared as a result of the bending performance test. As mentioned above, researchers revealed the advantages of timber-steel composite beams. However, the structural behavior of the hybrid beam was designed and analyzed in the elastic range.

When a GLT beam is glued with other materials (steel or fiber-reinforced polymer (FRP)) by an adhesive, the risk of glueline delamination has been reported (Metelli *et al*. 2016; Schober *et al*. 2015), and it is hard to expect good durability. Tomasi *et al*. (2009) tried to develop a ductile bending behavior of GLT beams by inserting steel bars. They showed that steel reinforcement provides a simple and reliable solution for robust timber structures. Wang *et al*. (2021) developed a glulam beam mechanically reinforced by a steel rod. They showed the possibility of ductile failure due to the yielding of glulam in compression parallel to the grain or yielding of the steel rod.

As mentioned above, most GLT-steel beams were developed by gluing GLT and steel. However, this study developed a separable glued-laminated timber (GLT)-steel beam without gluing as an eco-friendly solution to building construction. The GLT-steel beam was assembled using inclined screws without gluing, which enabled the easy separation of the materials for recycling purposes. The minimum thickness of steel for inducing compressive GLT failure was investigated, and the reinforcing effect and bending behavior of the developed GLT-steel beam were analyzed. Based on the experimental test, a prediction model for the load-carrying capacity of the GLT-steel beam has been developed.

DESIGN OF GLT-STEEL BEAM

Figure 1 shows schematically the concept of the separable GLT-steel beam. In this study, the GLT-steel beam is designed to fail by a universal test machine with a load capacity of 100 kN, based on the previous study (Pang *et al*. 2018). The load-carrying capacity of the GLT-steel composite beam was designed by applying the composite beam theory, under the assumption that GLT and steel are completely combined and linear elasticity materials. Figure 2 shows the load-carrying capacity, neutral axis position, and total thickness according to the steel plate thickness when a GLT (80 mm (width) × 120 mm (thickness) × 2450 mm (length)) is reinforced with steel plates. As the thickness of the steel plate increases, the thickness of the composite beam increases and the neutral axis goes down toward the bottom.

In the case of load-carrying capacity, as the thickness of the steel plate increased, the load that the composite beam could support also increased, but the increase rate of the

load decreased when the thickness was 4 mm or more. When GLT was reinforced with a steel thickness of 3 mm or less, the maximum load of the beam was governed by the tensile failure of the steel plate. However, when GLT was reinforced with a steel thickness of 4 mm or more, the maximum load of the beam was governed by compression failure of GLT. Therefore, in this study, the GLT was reinforced with a 4 mm thick steel plate to check whether compression fracture of GLT occurred.

Fig. 1. Separable glued-laminated timber-steel beam

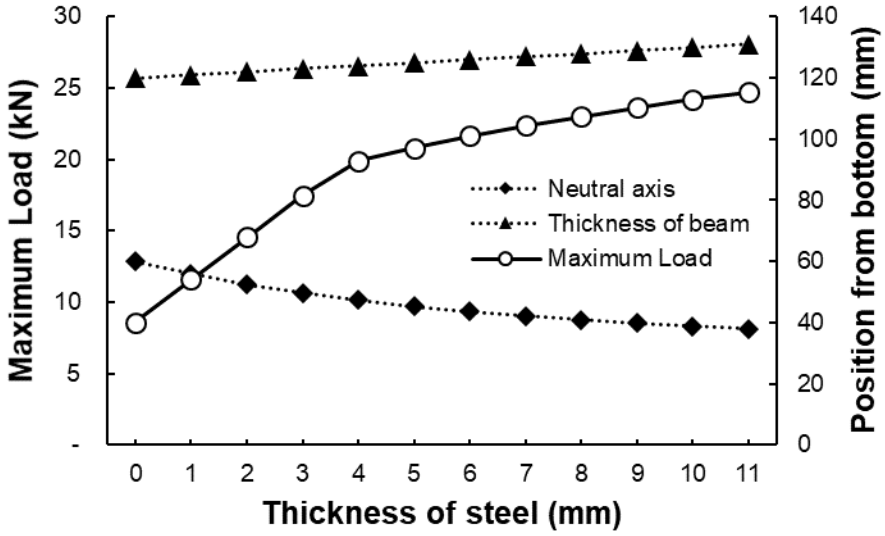

Fig. 2. Load-carrying capacity, neutral axis position, and total thickness of beam according to the steel plate thickness

EXPERIMENTAL

Materials

Figure 3 shows the cross section of GLT and the combination of lamina. One lamina grade (E9) was used, and the modulus of elasticity (MOE) of that grade was greater than 9 GPa. The GLTs were manufactured using four layers of larch species (*Larix kaempferi* Carr., the density of 550 kg/m^3) lamina according to the KS F3021 standard (KS F3021 2013). The size of GLT was 80 mm (width) × 120 mm (thickness) × 2450 mm (length). The GLT specimens were stored for one week in a bending test laboratory (20 °C, 65% R.H.). After the bending test, the moisture content of GLT was measured with a moisture tester (HM-530, Kett Electric Laboratory, Tokyo, Japan) and was about 6 ± 2%.

Table 1 shows the dimensions and mechanical properties of GLT and steel plate.

Eight GLTs were prepared, and all of the actual bending stiffness of the GLTs were measured. GLTs were divided into two groups to have similar bending stiffness. One group (3 out of 8) was used to measure the bending strength of GLT, and the other group (5 out of 8) was reinforced with a steel plate.

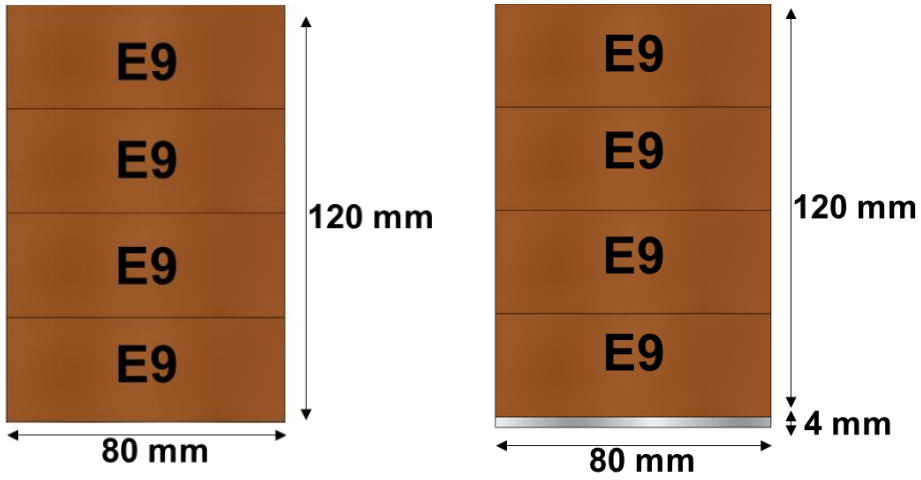

(a) GLT beam **(b)** GLT-steel

Fig. 3. Cross section of GLT and GLT-steel beam

Table 1. Dimensions and Mechanical Properties of GLT and Steel Plate

Material	Dimensions (mm)			Elastic Modulus (MPa)	Strength (MPa)
	Thickness	Width	Length		
GLT[1)]	120	80	2450	14443[2)]	Bending strength: 55.7[2)]
Steel Plate[3)]	4	80	2400	166330[4)]	Yield strength: 227[5)] Tensile strength: 345[5)]

[1)] Glued-laminated timber (KS F3021 2013)
[2)] Experimental value in this study
[3)] Steel Plate Hot Commercial (KS D3501 2018)
[4)] Experimental value from Suh *et al*. (Chang-Min and Hyun-Chul 2009)
[5)] Experimental value from mill test certificate

To reinforce the GLT, a 4 mm thick steel plate (Steel Plate Hot Commercial, SPHC (KS D3501 2018)) was installed at the bottom of the GLT. The steel plate and GLT were fixed with self-tapping screws (VGS Ø9 × 160mm (ETA-11/0030 2019)). Axial slip moduli of screws are significantly higher compared to slip moduli in shear (Dietsch and Brandner 2015). Thus, the screw was installed at an angle of 45° using a washer (HUS945, Rothoblaas) to minimize the slip between the GLT and the steel plate.

When the GLT is reinforced with a 4 mm steel plate, the maximum load of the composite beam is about 20 kN, and the shear force generated between the GLT and steel is 84.7 kN. The design value of the inclined screw used is 11.25 kN (Rotho Blaas Srl 2020) and 8 screws can support the shear force generated between the GLT and steel plate. However, 10 screws were installed at intervals of 60 mm to prevent the screw connector failure and to observe the bending failure of the GLT-steel beam. The axis of the screw was rotated 20 degrees toward the center of the GLT to prevent the GLT from being cracked by the screws, as shown in Fig. 4.

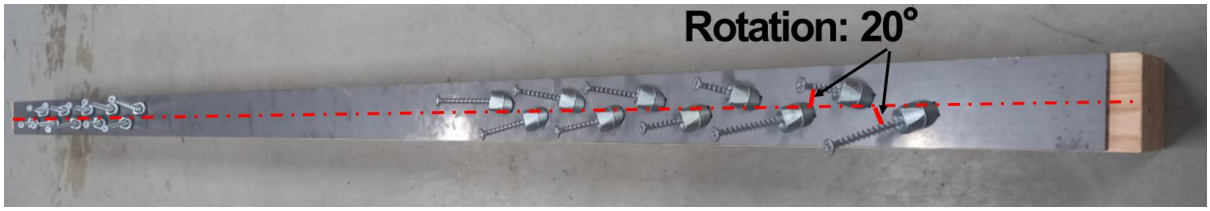

Fig. 4. Screw installation (45° inclined, 20° rotation)

Experimental Tests

The deflection and load resistance of specimens were measured by a third-point bending test to derive their bending stiffness and load-carrying capacities (Fig. 5). The load was applied using a universal test machine (Zwick GmbH & Co., Ltd., Ulm, Germany) according to ASTM D198 (2010). A yoke was installed on the neutral axis of the specimen to measure the pure deflection.

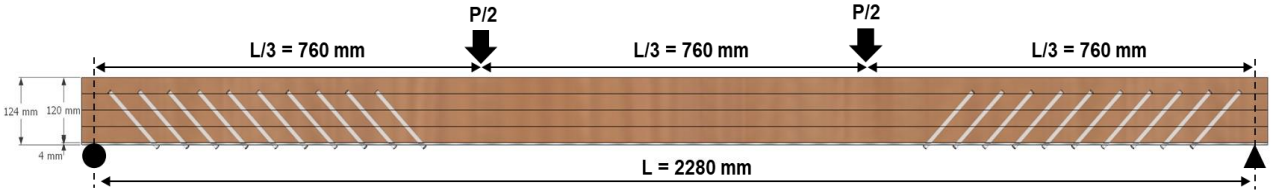

Fig. 5. Configuration of third-point loading test for the specimens

The actual displacement was measured at the center of the specimen using the linear variable displacement transducers (LVDT). The test span and the loading speed were 2,280 mm and 10 mm/min, respectively. The bending stiffness and bending moment of the specimens were calculated using Eq. 1 (BS EN 408:2010+A1:2012 2012; Pang *et al*. 2019; Pang and Jeong 2019) and Eq. 2, respectively,

$$(EI)_{test} = \frac{(P_2 - P_1) \cdot L_e \cdot (3L^2 - 4L_e^2)}{48 \cdot (d_2 - d_1)} \quad (1)$$

$$M_{measured} = \frac{P_{max}}{2} \cdot L_e \quad (2)$$

where $(EI)_{test}$ is the experimental bending stiffness of the specimen (N·mm^2), L_e is the distance between the load position and support positions (mm), L is the span of the specimen (mm), P_1 and P_2 are the loads corresponding to 10% and 40% of the maximum load, P_{max}, respectively (kN), d_1 and d_2 are the deflections corresponding to P_1 and P_2, respectively (mm), and $M_{measured}$ is the measured bending moment capacity (kN·m).

RESULTS

GLT Beam

Figure 6 shows the failure modes of the GLT beam. All specimens were broken around the knot in the tensile zone. At the time of failure, the load resistance dropped sharply, as shown in Fig. 7. This brittle failure is a typical failure mode of GLT or wood in bending tests (Pang *et al*. 2011, 2018, 2021; Pang and Jeong 2019).

Table 2 shows the bending properties of the GLT specimens. The average bending stiffness of the GLT in the failure test was 0.168×10^{12} N·mm^2, which was similar to the stiffness in the grading test. The average load-carrying capacity of the GLT was 28.2 kN, and the bending moment capacity was 10.7 kN·m.

(a) Tensile failure of the bottom lamina

(b) Tensile failure around knot at the bottom lamina

Fig. 6. Failure mode of the GLT beam

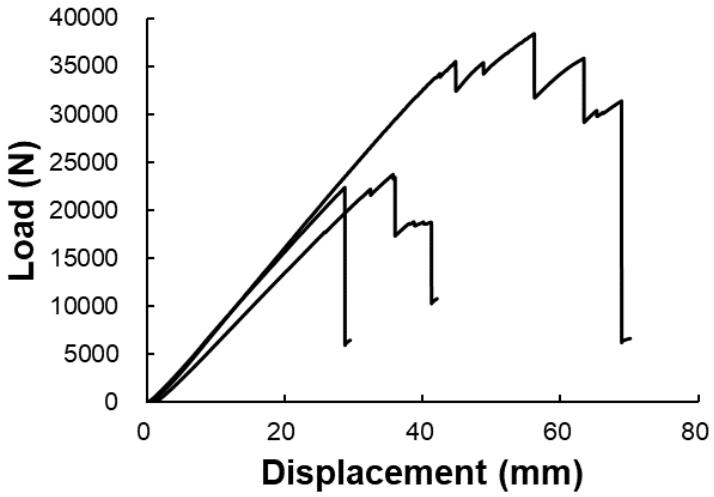

Fig. 7. Load-displacement curve of the GLT beam

Table 2. Bending Properties and Failure Modes of GLT and Reinforeced GLT

No.		EI_{eff} [1] (10^{12} N·mm^2)			Bending Moment Resistance		First Failure
		Grading test[2]	Failure test[3]	Ratio[4] (%)	P_{max}[5] (kN)	Moment[6] (kN·m)	
GLT beam	GLT-1	0.165	0.164	99.3	22.373	8.501	Tension (knot)
	GLT-2	0.155	0.151	97.2	23.720	9.013	Tension (knot)
	GLT-3	0.182	0.177	97.0	38.398	14.591	Tension (fiber)
	Average	0.168	0.164	97.9	28.164	10.702	
	COV[7]	0.067	0.065	0.011	0.258	0.258	
GLT-steel beam	RGLT-1	0.183	0.266	144.9	32.869	12.490	Tension (finger)
	RGLT-2	0.166	0.255	153.5	38.758	14.727	Tension (knot)
	RGLT-3	0.165	0.260	157.9	48.148	18.296	Compression
	RGLT-4	0.160	0.277	172.8	48.894	18.579	Compression
	RGLT-5	0.157	0.257	163.3	51.594	19.605	Compression
	Average	0.166	0.263	158.5	44.053	16.740	
	COV	0.054	0.030	0.059	0.161	0.161	

[1] Effective bending stiffness by Eq. 1
[2] Measured in grading test to divide the specimens into two groups.
[3] Measured in failure test to evaluate the maximum load-carrying capacity of the specimen
[4] (EI_{eff} in grading test / EI_{eff} in failure test) × 100
[5] Maximum load
[6] Bending moment resistance calculated by Eq. 2
[7] Coefficient of variation

GLT-steel beam

Figures 8 through 10 show the failure mechanism of the GLT-steel beam. In two of the five specimens, tensile failure occurred first at the finger joint (Fig. 8a) or knot (Fig. 9a) of GLT. The finger-joint and knots are the main factors causing the strength reduction (Pang *et al*. 2011, 2018, 2021; Pang and Jeong 2019). Unlike the GLT beam, compression failure occurred at the top of the GLT (Fig. 8b and Fig. 9b) and large deformation occurred (Fig. 8c and Fig. 9c).

In three of the five specimens, compressive failure occurred first at the top of the GLT (Fig. 10a). After that, tensile failure occurred at the knot, but the tensile failure of the specimens did not lead to rapid brittle failure. The specimens showed ductile behavior due to the elongation of the steel plate. As described in the material section, the number of screws was calculated and installed to sufficiently support the expected shear force between GLT and steel plate. During the experiment, no screw was pulled out, and no damage was found between the screw and the steel plate. Therefore, the elongation of the steel plate shows that the screw connection sufficiently supported the shear force between GLT and the steel plate.

Figure 11 shows the load-displacement curve of the GLT-steel beams. Unlike the GLT beam, the GLT-steel beam did not lose its load-carrying capacity significantly after the initial failure and maintained a load-carrying capacity of approximately 30 kN. This may be because the steel plate is in a plastic state in which the stress does not increase even

when the strain increases. The maximum load-carrying capacity was higher in the case where the compression failure occurred first (48 kN to 51 kN) than in the case where the tensile failure occurred first (32 to 38 kN). This shows that the tensile part (bottom of GLT) contributed to the load-carrying capacity of the GLT-steel beam until the tensile failure occurred.

(a) Tensile failure at finger joint of GLT

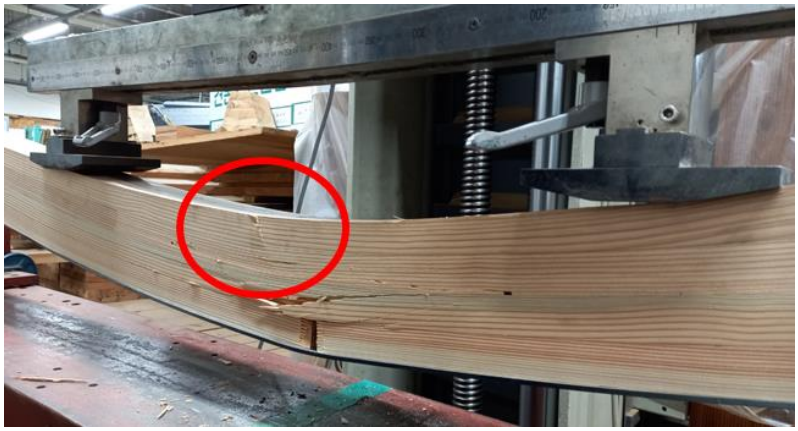

(b) Compression failure on top of GLT

(c) Large deformation

Fig. 8. Fracture mechanism of GLT-steel beam in which tension failure (finger joint) of GLT occurs first (RGLT-1)

(a) Tensile failure at knot of GLT

(b) Compression failure on top of GLT

(c) Large deformation

Fig. 9. Fracture mechanism of GLT-steel beam in which tension failure (knot) of GLT occurs first (RGLT-2)

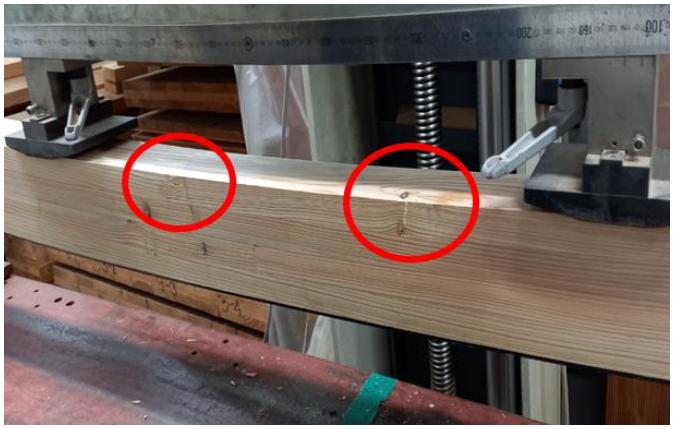

(a) Compression failure on top of GLT

(b) Tension failure on bottom of GLT

(c) Large deformation

Fig. 10. Fracture mechanism of GLT-steel beam in which compression failure of GLT occurs first

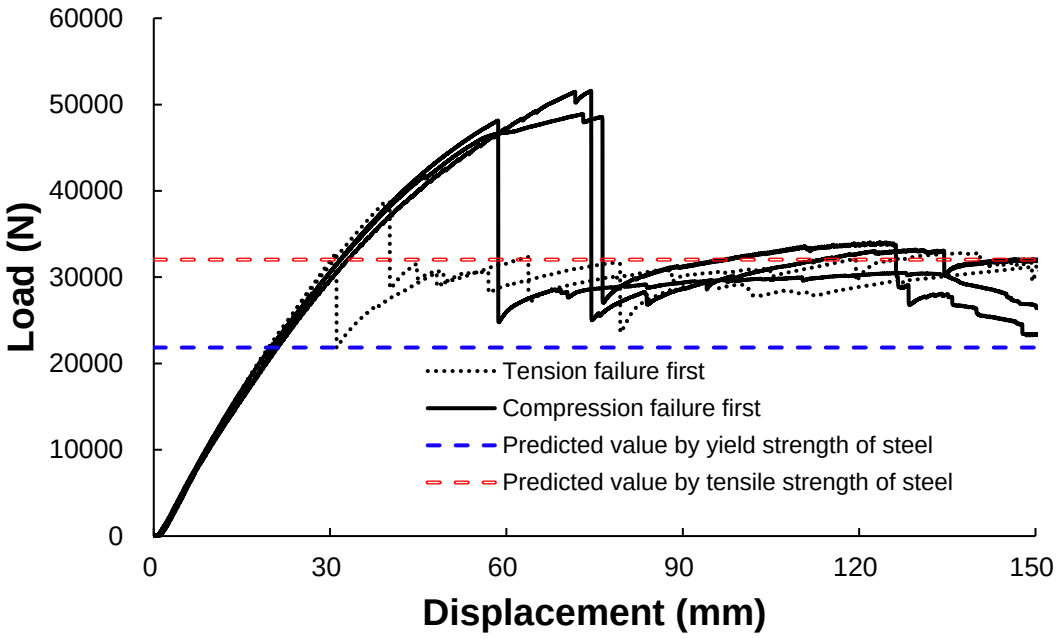

Fig. 11. Load-displacement curve of the GLT-steel beam

DISCUSSION

By reinforcing the GLT with a 4 mm steel plate, the bending stiffness was improved by about 58.5% from 0.166×10^{12} to 0.263×10^{12} N/mm^2, and the coefficient of variation (COV) decreased from 0.054 to 0.03 (Table 2). The bending moment resistance of the GLT-steel beam was increased by 56.4% from 10.702 to 16.740 kN·m, and the COV decreased from 0.258 to 0.161. Therefore, the GLT-steel beam developed in this study has high bending performance compared to general GLT and can be produced with uniform quality.

Figure 12 shows the bending stress distribution of the GLT beam and GLT-steel beam at the maximum bending moment. The bending stress distribution in Fig. 12 was plotted by elastic analysis (Eq. 3). The maximum bending stress of the GLT beam was 55.7 MPa, which was similar to the bending strength (54 MPa) of a GLT grade with similar MOE in KS F3021 standard (KS F3021 2013). In the case of the GLT-steel beam, however, the maximum bending stress acting on the steel plate (414.6 MPa, Fig. 12(b)) exceeded the yield strength of the used steel plate (227 MPa). This means that the steel plate was in a plastic state, and plastic analysis is required.

$$\sigma_{bending} = n \cdot \frac{M_{measured}}{I_{eff}} \cdot y \quad (3)$$

where $\sigma_{bending}$ is the bending stress in the elastic analysis (MPa), n is the ratio of elastic modulus of GLT and steel in GLT-steel beam (1 for GLT beam), $M_{measured}$ is the measured bending moment capacity (kN·m), I_{eff} is effective moment of inertia (mm^4), y is the distance from the neutral axis (mm).

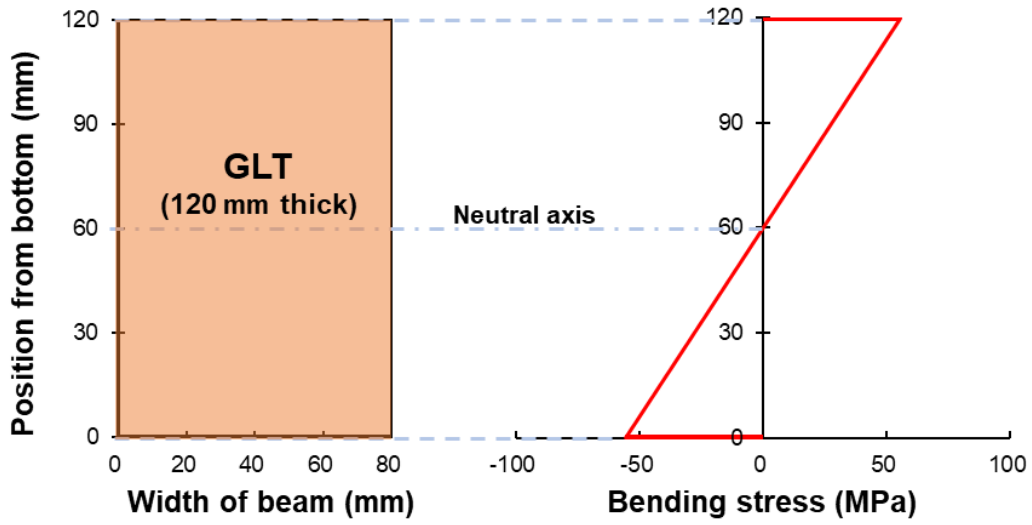

(a) GLT beam

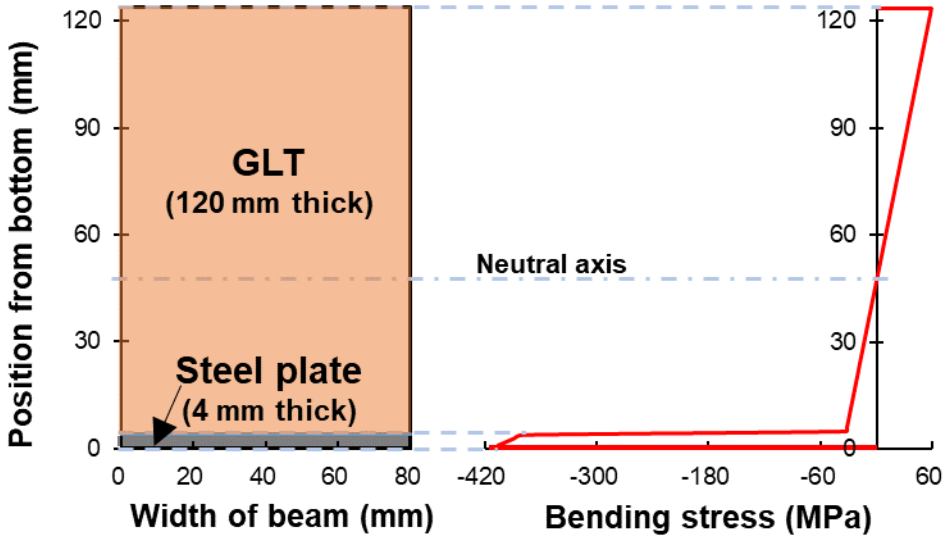

(b) GLT-steel beam (stress acting on steel exceeds the yield strength (227 MPa) of steel)

Fig. 12. Bending stress distribution of GLT beam and GLT-steel beam by elastic analysis

Figure 13 shows the bending stress distribution of GLT-steel beam considering the plasticity of the GLT and steel. The maximum bending moment of the GLT-steel beam can be predicted by Eq. 4. Equation 4 consists of three terms. The first term is the plastic bending moment of compression zone in GLT, the second term is the elastic bending moment in GLT, and the third term is the plastic bending moment of the steel plate. In the compression test of wood, the load-displacement curve shows a ductile behavior in which the strength decreases slowly as the wood wrinkles after the maximum load (Pang and Jeong 2018). For plastic analysis of GLT-steel beam, the load-displacement curve of GLT in compressive stress was idealized as an elastic-plastic curve. Tomasi *et al*. (2009) and Wang *et al*. (2021) also assumed the compressive behavior for the fiber direction in a GLT reinforced by steel rods as an elasto-plastic behavior. Among the reported experimental

data (Pang and Jeong 2018; Park *et al*. 2010), the compressive strength (58.8 MPa) of wood with similar elastic modulus in the same species was regarded as the yield strength of GLT,

$$M_{max} = \int_{c_1-h_{c,GLT}}^{c_1} \sigma_{c,GLT} \cdot y \, dA + \int_{c_2-t_{steel}}^{c_1-h_{c,GLT}} E_{GLT} \cdot \varepsilon_{GLT} \cdot y \, dA + \int_{c_2-t_{steel}}^{c_2} f_y \cdot y \, dA \quad (4)$$

where M_{max} is the maximum bending moment (kN·m), c_1 is the distance between the top surface and the neutral axis of the composite section (mm), $h_{c,GLT}$ is the height of the compressive zone in GLT (mm), $\sigma_{c,GLT}$ is the compressive strength of GLT (MPa), y is the distance from the neutral axis of the composite section (mm), c_2 is the distance between the bottom surface and the neutral axis of the composite section (mm), t_{steel} is the thickness of steel plate (MPa), E_{GLT} is the elastic modulus of GLT (MPa), ε_{GLT} is the strain of GLT, and f_y is the yield strength of steel plate (MPa).

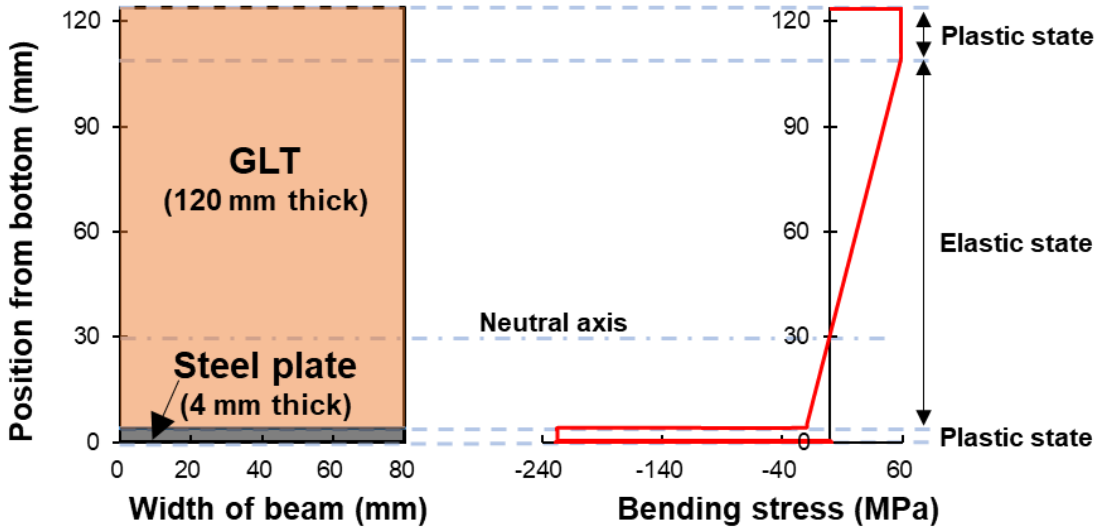

Fig. 13. Bending stress distribution of the GLT-steel beam at the maximum bending moment by elastic-plastic analysis

Figure 14 shows the bending stress distribution of the GLT-steel beam when the steel and timber in compressive zone reach plastic state. Assuming that the steel plate and the GLT are fixed and do not slide, the GLT-steel beam design method can be derived by considering the balance of compressive force and tensile force generated in the GLT-steel beam, similar to the reinforced concrete design method. The compressive force acting on the upper part of the GLT and the tensile force by the steel plate are equal according to the condition of equilibrium of compressive force and tensile force. Thus, the height of the compressive zone in the GLT-steel beam can be calculated by Eq. 5. Figures 14 (a) and (b) show when the maximum stress of steel reached the yield strength (227 MPa) and the maximum tensile strength (345 MPa) of the steel plate, respectively. When the maximum stress of the steel from yield strength to maximum tensile strength increased, the height of the compressive zone in the GLT-steel beam also increased.

The bending moment and the load-carrying capacity of the GLT-steel beam can be predicted by Eqs. 6, and 7, respectively. The predicted load-carrying capacity of GLT-steel beam was 21,845 N by applying yield strength of steel (227 MPa) and 32,035 N by applying yield strength of steel (345 MPa). Figure 11 shows the load-carrying capacity

predicted by Eq.7 together with the experimentally measured load-displacement curve. The load capacity predicted by the maximum tensile strength of the steel was similar to the maximum load capacities at the plastic condition of the test specimens. This indicates that the steel plate almost reached its maximum tensile strength. In addition, all of the load capacities of the test specimens were higher than the load predicted by the yield strength of steel. Therefore, the bending moment of GLT-steel beam can be safely designed with the yield strength of steel.

$$h_{c,GLT} = \frac{f_y \cdot t_{steel}}{\sigma_{c,GLT}} \quad (5)$$

$h_{c,GLT}$ is the the height of the compressive zone in GLT (mm), f_y is the yield or tensile strength of steel plate (MPa), t_{steel} is the thickness of steel plate (MPa), and $\sigma_{c,GLT}$ is the compressive strength of GLT (MPa).

$$M_{predict} = f_y \cdot w \cdot t_{steel} \cdot (h - \frac{t_{steel}}{2} - \frac{h_{c,GLT}}{2}) \quad (6)$$

In Eq. 6, $M_{predict}$ is the predicted bending moment (kN·m), f_y is the yield or tensile strength of steel plate (MPa), w is the width of steel plate (mm), t_{steel} is the thickness of steel plate (mm), h is the height of GLT-steel beam (mm), and $h_{c,GLT}$ is the height of compressive zone in GLT (mm).

$$P_{predict} = \frac{M_{predict}}{L_e} \cdot 2 \quad (7)$$

In Eq. 7, $P_{predict}$ is the predicted load-carrying capacity of GLT-steel beam (kN), $M_{predict}$ is the predicted bending moment (kN·m), and L_e is the the distance between the load position and support position (mm).

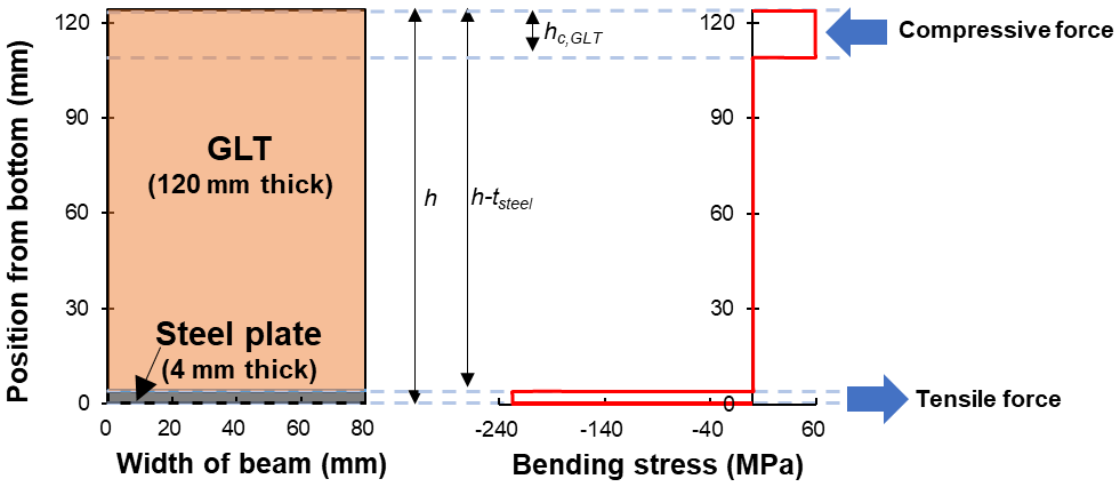

(a) Bending stress distribution at the yield strength (227 MPa) of the steel plate

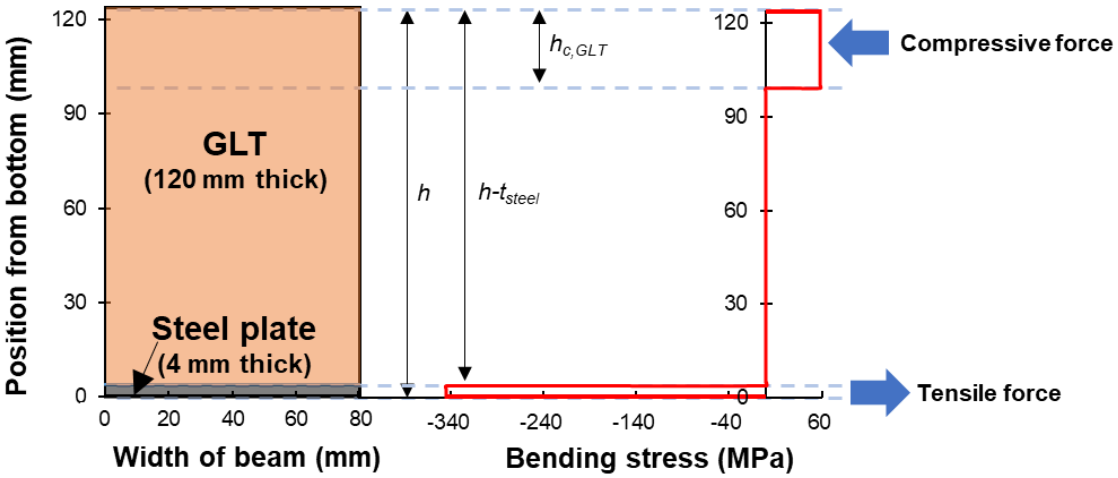

(b) Bending stress distribution at the tensile strength (345 MPa) of the steel plate

Fig. 14. Bending stress distribution of the reinforced GLT specimens at the plastic state

CONCLUSIONS

In this study, a separable GLT-steel beam was designed using the minimum steel plate thickness (4 mm) at which GLT experienced compressive failure, and the bending behavior was experimentally analyzed. The main findings are as follows.

1. The bending moment resistance and bending stiffness of the GLT-steel beam were improved by 56.4% and 58.5%, respectively, compared to the GLT beam. Additionally, the COV of both properties decreased. Thus, the GLT-steel beam developed in this study has the uniform quality and high bending performance compared to GLT.
2. The GLT-steel beam showed ductile behavior even after GLT failure and maintained a load resistance of about 30 kN during large deformation. The prediction model for the ductile behavior (plastic moment) was derived by considering the balance of the compressive forces and tensile forces in the composite beam, similar to the reinforced concrete design method. The experimentally measured load-carrying capacity of the beam was similar to the predicted load-carrying capacity. Therefore, the ductile behavior of the GLT-steel beam can be designed by the developed model.
3. The GLT and steel plate were mechanically connected using only inclined screws without the use of any adhesives. The resistance of the screw sufficiently supported the shear forces so that the steel plate can perform plastic behavior after yielding. Therefore, this study shows the possibility of a non-adhesive GLT-steel beam with plastic behavior.

ACKNOWLEDGMENTS

This research was supported by Basic Science Research Program through the National Research Foundation of Korea (NRF) funded by the Ministry of Education (No. NRF-2021R1I1A1A01045628).

REFERENCES CITED

André, A. (2006). *Fibres for Strengthening of Timber Structures*, Master Thesis, Luleå Tekniska Universitet, Civil and Environmental Engineering, Structural Engineering.

ASTM D198-15 (2010). "Standard test methods of static tests of lumber in structural sizes," ASTM International, West Conshohosken, PA, USA.

BS EN 408:2010+A1:2012 (2012). "Timber structures – Structural timber and glued laminated timber - Determination of some physical and mechanical properties," British Standards Institution, London.

Chang-Min, S., and Hyun-Chul, J. (2009). "Structural analysis of S-cam brake shoe for commercial vehicle by FEM," *J. Ocean Eng. Technol.* 23(4), 69-77.

Dietsch, P., and Brandner, R. (2015). "Self-tapping screws and threaded rods as reinforcement for structural timber elements – A state-of-the-art report," *Construction and Building Materials* 97, 78-89. DOI: 10.1016/j.conbuildmat.2015.04.028

ETA-11/0030. (2019). "European technical assessment. Screws for use in timber construction. ETA-Denmark, Nordhavn," ETA-11/0030. (2019). European technical assessment. Screws for use in timber construction. ETA-Denmark, Nordhavn.

Gerilla, G. P., Teknomo, K., and Hokao, K. (2007). "An environmental assessment of wood and steel reinforced concrete housing construction," *Building and Environment*, 42(7), 2778-2784. DOI: 10.1016/j.buildenv.2006.07.021

Hafner, A., and Schäfer, S. (2018). "Environmental aspects of material efficiency versus carbon storage in timber buildings," *European Journal of Wood and Wood Products*, 76(3), 1045-1059. DOI: 10.1007/s00107-017-1273-9

KS D3501 (2018). "Hot-rolled mild steel plates, sheets and strip," Korean Standards Association, Yeoksamdong, South Korea.

KS F3021 (2013). "Structural glued laminated timber," Korean Standards Association, Yeoksamdong, South Korea.

Lee, I. H., Song, Y. J., and Hong, S. I. (2021). "Tensile shear strength of steel plate-reinforced larch timber as affected by further reinforcement of the wood with carbon fiber reinforced polymer (CFRP)," *BioResources* 16, 5106-5117.

Li, J., Rismanchi, B., and Ngo, T. (2019). "Feasibility study to estimate the environmental benefits of utilising timber to construct high-rise buildings in Australia," *Building and Environment* 147, 108-120. DOI: 10.1016/j.buildenv.2018.09.052

Loss, C., Piazza, M., and Zandonini, R. (2016a). "Connections for steel-timber hybrid prefabricated buildings. Part I: Experimental tests," *Construction and Building Materials* 122, 781-795. DOI: 10.1016/j.conbuildmat.2015.12.002

Loss, C., Piazza, M., and Zandonini, R. (2016b). "Connections for steel-timber hybrid prefabricated buildings. Part II: Innovative modular structures," *Construction and Building Materials* 122, 796-808. DOI: 10.1016/j.conbuildmat.2015.12.001

Metelli, G., Preti, M., and Giuriani, E. (2016). "On the delamination phenomenon in the

repair of timber beams with steel plates," *Construction and Building Materials* 102, 1018-1028. DOI: 10.1016/j.conbuildmat.2015.09.038

Moritani, F. Y., Martins, C. E., and Dias, A. M. (2021). "A literature review on cold-formed steel-timber composite structures," *BioResources* 16, 1-20

Pang, S.-J., Park, J.-S., Hwang, K.-H., Jeong, G.-Y., Park, M.-J., and Lee, J.-J. (2011). "Bending strength of Korean softwood species for 120×180 mm structural members," *Journal of the Korean Wood Science and Technology* 39(5), 444-450. DOI: 10.5658/WOOD.2011.39.5.444

Pang, S.-J., Lee, J.-J., and Oh, J.-K. (2013). "Evaluation of allowable bending stress of dimension lumber; Confidence levels and size-adjustment," *Journal of the Korean Wood Science and Technology* 41(5), 432-439. DOI: 10.5658/WOOD.2013.41.5.432

Pang, S.-J., and Jeong, G. Y. (2018). "Load sharing and weakest lamina effects on the compressive resistance of cross-laminated timber under in-plane loading," *Journal of Wood Science* 64(5), 538-550. DOI: 10.1007/s10086-018-1741-9

Pang, S.-J., Oh, J.-K., Hong, J.-P., Lee, S.-J., and Lee, J.-J. (2018). "Stochastic model for predicting the bending strength of glued-laminated timber based on the knot area ratio and localized MOE in lamina," *Journal of Wood Science* 64(2), 126-137. DOI: 10.1007/s10086-017-1682-8

Pang, S. J., and Jeong, G. Y. (2019). "Effects of combinations of lamina grade and thickness, and span-to-depth ratios on bending properties of cross-laminated timber (CLT) floor," *Construction and Building Materials* 222, 142-151. DOI: 10.1016/J.CONBUILDMAT.2019.06.012

Pang, S.-J., Lee, H.-J., Yang, S. M., Kang, S. G., and Oh, J.-K. (2019). "Moment and shear capacity of ply-lam composed with plywood and structural timber under out-of-plane bending," *Journal of Wood Science* 65(1), 68. DOI:10.1186/s10086-019-1847-8Pang, S.-J., Lee, H.-J., Ahn, K.-S., and Oh, J.-K. (2020). "Sensitivity of censored data analysis to determine the characteristic value of structural timber," *Journal of Wood Science* 66(1), 39. DOI: 10.1186/s10086-020-01885-0

Pang, S.-J., Shim, K.-B., and Kim, K.-H. (2021). "Effects of knot area ratio on the bending properties of cross-laminated timber made from Korean pine," *Wood Science and Technology* 55(2), 489-503. DOI: 10.1007/s00226-020-01255-5

Pang, S.-J., Ahn, K.-S., Jeong, S., Lee, G.-C., Kim, H. S., and Oh, J.-K. (2022). "Prediction of bending performance for a separable CLT-concrete composite slab connected by notch connectors," *Journal of Building Engineering* 49, article 103900. DOI: 10.1016/j.jobe.2021.103900

Park, C.-Y., Pang, S.-J., Park, J.-S., Kim, K.-M., Park, M.-J., and Lee, J.-J. (2010). "Study of the distribution properties and LRFD code conversion in Japanese larch," *Journal of the Korean Wood Science and Technology* 38(2), 94-100. DOI: 10.5658/WOOD.2010.38.2.94

Petersen Raymer, A. K. (2006). "A comparison of avoided greenhouse gas emissions when using different kinds of wood energy," *Biomass and Bioenergy* 30(7), 605-617. DOI: 10.1016/j.biombioe.2006.01.009

Resch, E., Andresen, I., Cherubini, F., and Brattebø, H. (2021). "Estimating dynamic climate change effects of material use in buildings—Timing, uncertainty, and emission sources," *Building and Environment* 187. DOI: 10.1016/j.buildenv.2020.107399

Riola-Parada, F. (2016). *Timber-Steel Hybrid Beams for Multi-Storey Buildings*, Ph. D. Dissertation, Technische Universität Wien, Vienna, Austria. DOI: 10.34726/hss.2016.23820

Röck, M., Saade, M. R. M., Balouktsi, M., Rasmussen, F. N., Birgisdottir, H., Frischknecht, R., Habert, G., Lützkendorf, T., and Passer, A. (2020). "Embodied GHG emissions of buildings - The hidden challenge for effective climate change mitigation," *Applied Energy* 258. DOI: 10.1016/j.apenergy.2019.114107

Rotho Blaas Srl. (2020). *Screws and Connectors for Wood*, Cortaccia (BZ), Italy

Sandanayake, M., Lokuge, W., Zhang, G., Setunge, S., and Thushar, Q. (2018). "Greenhouse gas emissions during timber and concrete building construction —A scenario based comparative case study," *Sustainable Cities and Society* 38, 91-97. DOI: 10.1016/j.scs.2017.12.017

Schober, K.-U., Harte, A. M., Kliger, R., Jockwer, R., Xu, Q., and Chen, J.-F. (2015). "FRP reinforcement of timber structures," *Construction and Building Materials* 97, 106-118. DOI: 10.1016/j.conbuildmat.2015.06.020

Tomasi, R., Parisi, M. A., and Piazza, M. (2009). "Ductile design of glued-laminated timber beams," *Practice Periodical on Structural Design and Construction* 14(3), 113-122. DOI: 10.1061/(ASCE)1084-0680(2009)14:3(113)

Tsai, M.-T., and Le, T. (2018). "Determination of initial stiffness of timber-steel composite (TSC) beams based on experiment and simulation modeling," *Sustainability* 10(4), 1220. DOI: 10.3390/su10041220

Wang, T., Wang, Y., Crocetti, R., Franco, L., Schweigler, M., and Wålinder, M. (2021). "An innovative timber-steel hybrid beam consisting of glulam mechanically reinforced by means of steel rod: Analytical and preliminary numerical investigations," *Journal of Building Engineering* 43, 102549. DOI: 10.1016/j.jobe.2021.102549

Wu, S., Shan, Q., Zhang, J., Tong, K., and Li, Y. (2021). "Shear behavior of I-shaped wood-steel composite beams," *BioResources* 16, 583-596.

Yan, H., Shen, Q., Fan, L. C. H., Wang, Y., and Zhang, L. (2010). "Greenhouse gas emissions in building construction: A case study of One Peking in Hong Kong," *Building and Environment* 45(4), 949-955. DOI: 10.1016/j.buildenv.2009.09.014

Article submitted: February 15, 2023; Peer review completed: March 11, 2023; Revised version received and accepted: April 7, 2023; Published: April 18, 2023.
DOI: 10.15376/biores.18.2.3838-3855